Instability and Morphology of Thin Liquid Films on Chemically Heterogeneous Substrates

Rahul Konnur, Kajari Kargupta, and Ashutosh Sharma*

Department of Chemical Engineering, Indian Institute of Technology, Kanpur, India 208 016

(Received 14 October 1999)

A new mechanism for the surface instability and dewetting of thin films on chemically heterogeneous substrates is identified and simulated. The time scale for instability varies inversely with the potential difference due to the heterogeneity. Heterogeneities can even destabilize spinodally stable films, reduce the time of rupture substantially for thicker films, and produce complex and locally ordered morphological features (e.g., ripples and castle-moat structures, lack of undulations before hole formation) that are not predicted by the spinodal mechanism.

PACS numbers: 68.15.+e, 47.20.Ma, 47.54.+r, 68.45.–v

Ultrathin fluid films (e.g., coatings) on solid substrates have attracted widespread interest in recent years [1–16]. The current theoretical understanding of thin film stability, dynamics, and morphology is limited to films on chemically homogeneous substrates. Such films are rendered unstable by a spinodal mechanism whenever the excess intermolecular interaction energy per unit area (ΔG) shows positive curvature with respect to the film thickness, h, e.g., when the effective Hamaker constant, A_s is positive for the long-range van der Waals interaction. Deliberately tailored chemically heterogeneous substrates are increasingly being used to engineer desired nano- and micropatterns in thin films [17]. Also, experiments even on the substrates that were thought to be relatively homogeneous show remarkable departures from the theory of spinodal dewetting [5–7,9]. These observations have repeatedly suggested the involvement of heterogeneous sites, e.g., dust, trapped microcavities, chemical contamination, variation of oxide layer thickness on silicon, variable chain adsorption, etc., all of which generate localized patches of surface properties or potential different from the surrounding substrate, as shown in Fig. 1. This Letter proposes and simulates a new mechanism of thin film instability and its evolution on chemically heterogeneous substrates. The general dynamical and morphological features of the instability are then clearly contrasted with the spinodal dewetting. One of our main results is that the heterogeneities, even on length scales substantially smaller than the spinodal scales can greatly accelerate the growth of surface instabilities and can even engender the rupture of spinodally stable films.

The following nondimensional thin film equation governs the stability and spatiotemporal evolution of a thin film system subjected to the excess intermolecular interactions (where $\Phi = [2\pi h^2/|A_s|][\partial \Delta G/\partial H]$):

$$\partial H/\partial T + \nabla \cdot [H^3 \nabla(\nabla^2 H)] - \nabla \cdot [H^3 \nabla \Phi] = 0. \quad (1)$$

Here $H(X, Y, T)$ is the nondimensional local film thickness scaled with the mean thickness h; γ and μ refer to the film surface tension and viscosity, respectively; X, Y are the nondimensional coordinates in the plane of the substrate, scaled with a characteristic length scale $(2\pi\gamma/|A_s|)^{1/2}h^2$; and the nondimensional time T is scaled with $12\pi^2\mu\gamma h^5/A_s^2$ (dimensional time is t).

Flow of fluid occurs in the direction of decreasing force per unit area, Φ. For homogeneous substrates, $\Phi = \Phi(H)$, and the spinodal dewetting is caused by flow from thinner to thicker regions only when $\partial\Phi/\partial H < 0$. The linear stability analysis of Eq. (1) provides the following spinodal length and time scales for the growth of instability: $\lambda_m^2 = -8\pi^2\gamma/(\partial^2\Delta G/\partial h^2)$ and $t_s = 12\mu\gamma/h^3(\partial^2\Delta G/\partial h^2)^2$ [18].

Nonlinear simulations have verified the above and established the following hallmarks of the spinodal dewetting: (a) initially, a strongly correlated, small amplitude undulating pattern emerges, (b) dewetting eventually occurs by the formation of circular holes or by the formation of bicontinuous undulations/droplets for relatively thick and thin films, respectively [4]. However, on a heterogeneous substrate, where $\Phi = \Phi(H, X, Y)$, another mode of surface instability driven by the gradient of force, $\nabla\Phi$, is also present even at constant film thickness. This microscale wettability contrast causes a flow from the less wettable (higher pressure) to more wettable (lower pressure) regions, even when the spinodal stability condition, $\partial\Phi/\partial H > 0$, is satisfied everywhere. This mechanism is analogous to the Marangoni flow, except that it derives from the gradient of free energy at the solid-film interface rather than at the free film surface. The same phenomenon is responsible for the climbing of a macroscopic drop on a substrate with wettability gradients [19].

For the sake of illustration, we consider a fairly general representation of antagonistic (attractive/repulsive) long- and short-range intermolecular interactions [4,18] on both the substrate (properties $[A_s, S_s^P]$) and the heterogeneous

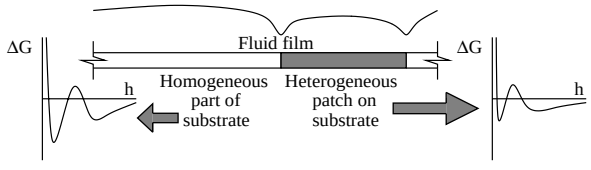

FIG. 1. Schematic diagram of the thin film system.

patch (properties $[A_h, S_h^P]$), where S^P represents the strength of the non–van der Waals interactions [6].

$$\Delta G = -(A/12\pi h^2) + S^P \exp(-h/l_p). \qquad (2)$$

As an example (see potentials in Fig. 1), the above potential represents liquid crystal films on silicon substrates when the effective Hamaker constant, A, and S^P, are both positive (long-range apolar van der Waals attraction combined with a shorter-range polar repulsion) [6]. Relatively thick and thin films of such a system are both spinodally unstable (since $\partial\Phi/\partial H < 0$), but the intermediate thickness films satisfying $\partial\Phi/\partial H > 0$ are spinodally stable. A true dewetting occurs for relatively thin films in the primary minimum ($h \to 0$), whereas for relatively thick films, pseudodewetting occurs in the secondary minimum of the free energy, h_* [18]. Simulations are reported for a few sets of parameters [20] chosen to illustrate the important phenomena while keeping some contact with a recent set of experiments [6]. However, based on extensive simulations with many different sets of parameters and functional forms of the potential (samples of which are reported in this Letter), we have confirmed all of the key conclusions reported here regarding the dynamics and morphology on heterogeneous substrates. Heterogeneous patches with diffused, rather than sharp boundaries, as well as noncircular boundaries also did not present any new physics. These details will be presented elsewhere.

Equation (1) was numerically solved using a central differencing scheme in space combined with Gears algorithm for stiff equations for time marching. The effect of heterogeneity is most clearly reflected in the morphology even during the very early stages of evolution as summarized in Fig. 2 for a 40 nm thick film. On a homogeneous surface, (pseudo-) dewetting occurs by the formation of an undulating structure with a characteristic spinodal length scale, λ_m [Fig. 2(a)]. In contrast, on a heterogeneous substrate, a very rapid deformation of the film surface occurs near the boundary of the patch leading to the formation of a localized hole, at which time the film surface away from the hole remains undisturbed and flat [Fig. 2(b)]. The time of rupture is reduced by 2 orders of magnitude compared to spinodal time t_s by the presence of heterogeneity in this case. The surface undulations characteristic of the spinodal mechanism appear and evolve on the homogeneous part of the substrate at a much later time. The primary contact line at the base of the hole remains pinned at the substrate-patch boundary. This feature seen in experiments [6] does not exist on homogeneous surfaces, where holes, once produced, continue to expand. At very long (spinodal) times, a thicker equilibrium film (secondary contact line) can partially evolve on the homogeneous part of the substrate giving a layered appearance to the hole.

We found that the time of rupture on a heterogeneous patch is independent of the length scale of the patch, as long as its length exceeds a critical value, which is at least an order of magnitude smaller than the spinodal length scale. For example, the spinodal length scales for 40, 70, and 100 nm films are 57, 175, and 360 μm, respectively, but rupture can be induced by a patch as small as 3 μm. Figure 3 compares the rupture time, t_n ($= t/\mu$), from the heterogeneous mechanism and the spinodal mechanism, both determined based on simulations. The gradient in wettability increases from curves 2 to 4 of Fig. 3. For the homogeneous system (curve 1 of Fig. 3), the dependence is in accord with the spinodal theory, $t_s \propto h^5$. In contrast, the thickness dependence of the characteristic time is weaker for the heterogeneous systems and decreases to $h^{3.2}$ for curve 4 of Fig. 3.

When the spinodal effects are weak $[(\partial\phi/\partial h) \times (\partial h/\partial x) \ll \partial\phi/\partial x|_h]$, a simple scaling analysis of Eq. (1) leads to the following characteristic time for the growth of instability by the heterogeneous mechanism: $t_h \propto 1/\Delta\phi$, where $\Delta\phi = (\phi_s - \phi_h)$ is the potential difference across the heterogeneous boundary evaluated at the initial thickness. The best fit to simulations ($|\Delta\phi/\phi_s| > 0.5$) indeed showed the ratio of the heterogeneous to spinodal time scales, $t_h/t_s = c|\phi_s/\Delta\phi|$, $c = 0.12$ and 0.094 for 40 and 100 nm thick films, respectively. The dependence on $\Delta\phi$ is more complicated for weaker wettability contrasts ($|\Delta\phi/\phi_s| < 0.5$), where

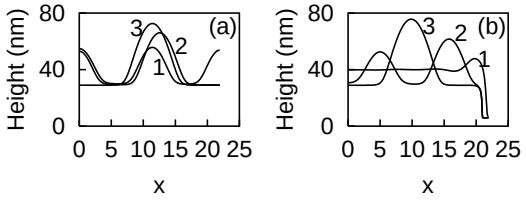

FIG. 2. Evolution of surface instability in a 40 nm thick film: (a) shows evolution on a homogeneous substrate. Curves 1, 2, and 3 show the profiles at the following times: $t_n = 1.73 \times 10^5$, 1.26×10^6, 1.67×10^{12} m s^2/kg, respectively; (b) is evolution on a chemically heterogeneous substrate with a heterogeneous patch of 1 μm length in the right-hand corner. Curves 1, 2, and 3 show the profiles at the following times: $t_n = 4.63 \times 10^3$, 1.36×10^5, 4.44×10^{11} m s^2/kg, respectively.

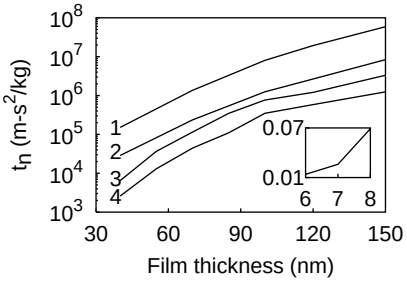

FIG. 3. Dependence of rupture time on film thickness for homogeneous (curve 1) and different heterogeneous systems (curves 2–4) with increasing wettability contrast from curves 2 to 4 [20]. The inset shows the time of rupture for films that are spinodally stable.

the spinodal mechanism also assists the evolution of instabilities.

3D simulations provide additional morphological features that can be compared with experiments. Figure 4 describes the evolution when the heterogeneity is *more* wettable than the surrounding substrate. A novel morphological feature is the formation of a droplet at the hole center giving a castle-moat appearance. This feature, frequently seen in experiments [1,6], always forms regardless of whether the patch is more or less wettable, whenever rupture is initiated at the patch boundary rather than at the center. At longer times [Fig. 4(C)], the hole rim, as well as the liquid ridges on the surroundings, breaks up to form droplets due to the Rayleigh instability and ripening. The initial signature of the heterogeneity is completely obliterated after this time [Fig. 4(D)].

Some of the novel characteristic 3D morphologies some time after the onset of spinodal dewetting regime are summarized in Fig. 5 for films of different thickness. Figure 5(A) shows a mixed morphology arising from the formation of a hole (on the heterogeneous patch) and the growth in the amplitude of undulations (on the surrounding homogeneous substrate). A similar pattern has been observed in experiments on liquid crystal films on silicon substrate [6]. Pictures 5(B) to 5(D) show a local ordering of the pattern that can extend to the homogeneous part, but it is initiated by a central heterogeneity, resulting in "ripples" and "flowers" which are sometimes witnessed in experiments. The instability in these cases is initiated by the formation of a ringlike depression [e.g., Fig. 5(B) and 5(C)], or by many tiny depressions/holes along the patch boundary [e.g., in Fig. 5(D)]. In the latter case, a rapid coalescence occurs to form again a ringlike depression. The depression is flanked by some trapped liquid at the center and an elevated rim. The side of the rim where it joins the undisturbed film undergoes local thinning [e.g., the depletion zone surrounding the outermost rim in Fig. 5(D)] [21,22]. This local thinning provides the preferred site for the formation of more depressions by the spinodal mechanism [e.g., Fig. 5(B)] resulting in an ordered arrangement, e.g., ripples. The process of ordering continues until the spinodal structures start appearing on the surroundings [e.g., Fig. 5(C)]. Thus, ordering is more prominent and longer ranged for thicker films, since the spinodal time scale increases more rapidly with the film thickness and becomes much larger than the heterogeneous time scale for thick films [e.g., curve 4 of Fig. 3, Fig. 6(b)].

To show the invariance of the above results with the form of the potential, we also simulated the inverse case characterized by a long-range repulsion combined with a shorter-range attraction as shown in Fig. 6(a). This potential mimics the behavior of polystyrene films on an oxide (low-energy) covered silicon (high-energy) substrate [5] and also the behavior of aqueous films on most solid surfaces [8,13]. For illustration, the heterogeneity is assumed to arise due to a local change in the thickness of the oxide layer [2.5 nm for the homogeneous substrate, curve 2 of Fig. 6(a); and 4 nm for the heterogeneous patch, curve 1 of Fig. 6(a)]. Films thicker than 6.8 nm are *spinodally stable* both on the homogeneous substrate and on the heterogeneous patch since its length is smaller than the critical length scale λ_c ($= \lambda_m/\sqrt{2}$) of the spinodal mechanism. Figure 6(b) compares the rupture time due to the spinodal and heterogeneous mechanisms. The surface tension of polymer film (γ) has been taken to be 38 mJ/m^2. Even spinodally stable films rupture rapidly due to heterogeneity. As before, a best fit to the data reveals $t_h/t_s = c|\phi_s/\Delta\phi|$, $c = 0.435$ and 0.044 for 4 and 6 nm thick films, respectively.

The thinnest films in the spinodal range ($<$6.8 nm) show mixed morphology [Fig. 7(A)] and local ordering [Fig. 7(B)]. For the thicker films, the spinodal evolution shifts from undulations to holes, giving rise to patterning of spinodally created holes around a heterogeneously created hole [Fig. 7(C)]. In these cases, the mean spinodal length scale over a large area is not greatly altered if the number of heterogeneous patches is not excessive. A most interesting heterogeneous phenomenon occurs outside the spinodal range, where the film should be stable were it not for the flow created by the heterogeneity. These relatively thick films continue to rupture by the formation of expanding localized holes [e.g., Fig. 7(D)].

As in the case of model PS films above, our simulations (not shown) again confirm that even relatively thick water films in the spinodally stable region can rupture due to the presence of small (0.1 μm) hydrophobic sites, e.g., due to oily contamination, as seen in experiments [8,13].

In conclusion, the presence of chemical heterogeneities even on length scales substantially smaller than the spinodal length scale can destabilize and rupture a thin film

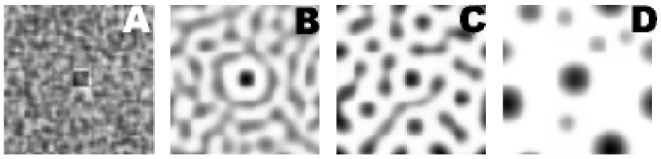

FIG. 4. Morphological evolution in a 40 nm thick film with a centrally located heterogeneous patch of greater wettability than the surroundings. In this, as well as in the subsequent images, a continuous linear gray scale between the minimum and the maximum thickness in each picture has been used.

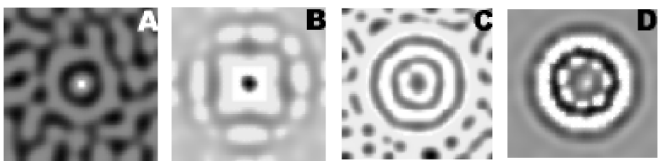

FIG. 5. Characteristic 3D morphology at late stages of evolution for films of thickness (A) 40 nm, (B) 70 nm, (C) and (D) 45 nm. The heterogeneous patch is at the center [20].

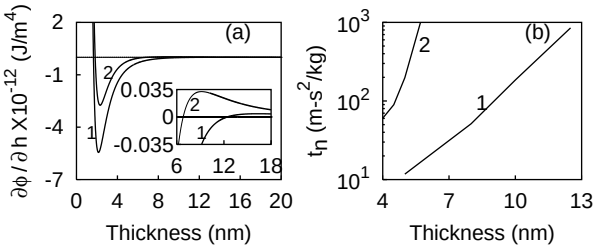

FIG. 6. (a) Variation of the spinodal parameter for a model polystyrene film on an oxide covered silicon wafer; (b) variation of the rupture time with film thickness. Curve 1: heterogeneous patch; curve 2: homogeneous substrate.

by engendering a gradient of chemical potential along the solid-liquid interface. The stronger flow in this heterogeneous mechanism is derived from a spatially fixed microscale-wettability contrast, rather than from temporally evolving local variations in the film thickness, as in the homogeneous-spinodal theory. Thus even spinodally stable thick films can undergo true rupture if the local thickness is initially reduced by the heterogeneous mechanism to a point where the spinodal condition is satisfied, and the two mechanisms achieve a cooperative effect thereafter. The time scale of heterogeneous instability can be many orders of magnitude smaller than that for a spinodal process and shows weaker dependence on the film thickness as compared to the spinodal time scale. Thus, the heterogeneous mechanism becomes most prominent for relatively thick films, in which a local ordering of pattern initiated by the heterogeneity can result. Simulations also reveal that the following morphological features, when they evolve in an initially uniform film, contain a clear-cut signature of the presence of heterogeneities: (a) absence of surface undulations prior to the birth of a hole, (b) formation of a nongrowing hole on a completely wettable surface or in a spinodally stable film, (c) mixed or distinct morphologies on different parts of the substrate, (d) a castle-moat pattern where a central drop is surrounded by a ringlike depression/hole, (e) a local ordering of the structure in which alternating layers of holes/depressions and ridges are formed. It is hoped that this study will aid in assessing the role of heterogeneities in thin film experiments where many of the above features are frequently witnessed [5–10,14], and will also help in the design of thin film experiments on patterned substrates.

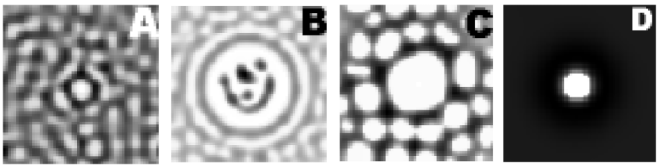

FIG. 7. The images in (A) and (B) are for a fixed 3 nm thick film, but a larger patch in (B) engenders more local ordering of the pattern. The image in (C) is for a 5 nm thick film; the image in (D) is for 13 nm thick spinodally stable film.

Useful discussions with G. Reiter, S. Herminghaus, K. Jacobs, and A. Karim are gratefully acknowledged. This work was supported by the Indo-French Centre for the Promotion of Advanced Research.

*Corresponding author.

[1] G. Reiter *et al.*, Langmuir **15**, 2551 (1999).
[2] H. I. Kim *et al.*, Phys. Rev. Lett. **82**, 3496 (1999).
[3] M. Sferrazza *et al.*, Phys. Rev. Lett. **81**, 5173 (1998).
[4] A. Sharma and R. Khanna, Phys. Rev. Lett. **81**, 3463 (1998); J. Chem. Phys. **110**, 4929 (1999).
[5] R. Xie *et al.*, Phys. Rev. Lett. **81**, 1251 (1998).
[6] S. Herminghaus *et al.*, Science **282**, 916 (1998).
[7] K. Jacobs, S. Herminghaus, and K. R. Mecke, Langmuir **14**, 965 (1998).
[8] U. Thiele, M. Mertig, and W. Pompe, Phys. Rev. Lett. **80**, 2869 (1998).
[9] T. G. Stange, D. F. Evans, and W. A. Hendrickson, Langmuir **13**, 4459 (1997).
[10] J. Kressler, C. Wang, and H. W. Kammer, Langmuir **13**, 4407 (1997).
[11] J. Bischof *et al.*, Phys. Rev. Lett. **77**, 1536 (1996).
[12] G. Reiter, Macromolecules **27**, 3046 (1994).
[13] M. Elbaum and S. Lipson, Phys. Rev. Lett. **72**, 3562 (1994).
[14] J. M. Guerra, M. Srinivasarao, and R. S. Stein, Science **262**, 1395 (1993).
[15] W. Zhao *et al.*, Phys. Rev. Lett. **70**, 1453 (1993).
[16] G. Reiter, Phys. Rev. Lett. **68**, 75 (1992); Langmuir **9**, 1344 (1993).
[17] H. Gau *et al.*, Science **283**, 46 (1999); P. Lenz and R. Lipowsky, Phys. Rev. Lett. **80**, 1920 (1998).
[18] A. Sharma and A. T. Jameel, J. Colloid Interface Sci. **161**, 190 (1993); A. Sharma, Langmuir **9**, 861 (1993).
[19] M. K. Chaudhuri and G. M. Whitesides, Science **256**, 1539 (1992).
[20] Results shown in Fig. 2 (curves 1 and 3), in the inset of Fig. 3, and in 5(A) and 5(B) are reported for the following parameters: substrate ($A_s = 1.06 \times 10^{-20}$ J, $S_s^P = 6.39$ mJ/m^2, $l_p = 2.5$ nm; which gives $h_* = 28.1$ nm); heterogeneity ($A_h = 2.12 \times 10^{-20}$ J, $S_h^P = 0.56$ mJ/m^2, and $l_p = 1.5$ nm; which gives $h_* = 5.8$ nm). For curve 2 of Fig. 3, $A_h = 2.12 \times 10^{-20}$ J, $S_h^P = 6.39$ mJ/m^2 and $l_p = 2.5$ nm and for curve 4 of Fig. 3, $A_h = 3.18 \times 10^{-20}$ J, $S_h^P = 1.68$ mJ/m^2, and $l_p = 1.5$ nm). For Fig. 4, $A_h = 0.18 \times 10^{-20}$ J, $S_h^P = 1.00$ mJ/m^2, and $l_p = 2.5$ nm. For Fig. 5(c): substrate: $A_s = 3.53 \times 10^{-21}$ J, $S_s^P = 2.13$ mJ/m^2, $l_p = 2.5$ nm; heterogeneity: $A_h = 1.765 \times 10^{-21}$ J, $S_h^P = 1.065$ mJ/m^2, $l_p = 2.0$ nm). For Fig. 5(d): substrate: $A_s = 7.06 \times 10^{-21}$ J, $S_s^P = 4.26$ mJ/m^2, $l_p = 2.5$ nm; heterogeneity: $A_h = 8.48 \times 10^{-21}$ J, $S_h^P = 2.56$ mJ/m^2, $l_p = 2.0$ nm. In all the above simulations, $\gamma = 72.8$ mJ/m^2.
[21] A. Ghatak, R. Khanna, and A. Sharma, J. Colloid Interface Sci. **212**, 483 (1999).
[22] G. Reiter, P. Auroy, and L. Auvray, Macromolecules **29**, 2150 (1996).